



## Article

# Recycled Carbon Black/High-Density Polyethylene Composite from Waste Tires: Manufacturing, Testing, and Aging Characterization

Catherine Billotte <sup>1,2</sup> , Laurence Romana <sup>2</sup>, Anny Flory <sup>2</sup>, Serge Kaliaguine <sup>3</sup>  and Edu Ruiz <sup>1,\*</sup>

<sup>1</sup> Département de Génie Mécanique, Polytechnique Montréal, C.P. 6079, succ. Centre-Ville, Montréal, QC H3C 3A7, Canada

<sup>2</sup> Groupe de Technologie des Surfaces et Interfaces, Département de Physique, Université des Antilles, Campus de Fouillole, Pointe à Pitre Cedex 97159, Guadeloupe

<sup>3</sup> Département de Génie Chimique, Université Laval, 1065 Avenue de la Médecine, Québec, QC G1V 0A6, Canada

\* Correspondence: edu.ruiz@polymtl.ca

**Abstract:** This study addresses the global issue of recycling used vehicle tires, typically burned out or trimmed to be reused in playground floors or road banks. In this study, we explore a novel environmentally responsive approach to decomposing and recovering the carbon black particles contained in tires (25–30 wt.%) by vacuum pyrolysis. Given that carbon black is well known for its UV protection in plastics, the objective of this research is to provide an ecological alternative to commercial carbon black of fossil origin by recycling the carbon black (rCB) from used tires. In our research, we create a composite material using rCB and high-density polyethylene (HDPE). In this article, we present the environmental aging studies carried out on this composite material. The topographic evolution of the samples with aging and the oxidation kinetics of the surface and through the thickness were studied. The Beer–Lambert law is used to relate the oxidative index to the characteristic depth of the samples. The UV photons are observed to penetrate up to 54% less with the addition of 6 wt.% of rCB compared to virgin HDPE. In this work, the addition of rCB as filler for HDPE used for outdoor applications has demonstrated to be an antioxidant for UV protection and a good substitute for commercial carbon black for industrial goods.

**Keywords:** HDPE; recycled carbon black; pyrolysis; photooxidation; FTIR; oxygen diffusion; accelerated aging



**Citation:** Billotte, C.; Romana, L.; Flory, A.; Kaliaguine, S.; Ruiz, E. Recycled Carbon Black/High-Density Polyethylene Composite from Waste Tires: Manufacturing, Testing, and Aging Characterization. *Recycling* **2024**, *9*, 107. <https://doi.org/10.3390/recycling9060107>

Academic Editor: Francesco Paolo La Mantia

Received: 16 August 2024

Revised: 26 September 2024

Accepted: 18 October 2024

Published: 5 November 2024



**Copyright:** © 2024 by the authors. Licensee MDPI, Basel, Switzerland. This article is an open access article distributed under the terms and conditions of the Creative Commons Attribution (CC BY) license (<https://creativecommons.org/licenses/by/4.0/>).

## 1. Introduction

Nearly one billion tires are manufactured worldwide each year, and this number continues to increase as our society continues to grow, which makes recycling of waste tires a constant challenge [1,2]. Even if recycling by trimming and recovery is performed in numerous countries, millions of tires are still being dumped in large landfills, and, if improperly managed, they may cause rubber pollution. Their accumulation presents significant risks, and the probability of fire is high, leading to environmental disasters. The life cycle assessment has demonstrated that the most polluting of the tire is not its manufacture but its end of life; a tire contains more than one hundred raw materials, most of which are not biodegradable [3]. It is therefore fundamental to develop alternatives allowing the recycling and recovery of waste tires from an environmental perspective. In developed countries the recycling industry has adopted granulation (e.g., production of stabs, field turf, or rubber fillers) or the use of tires as fuel for their high energy value in combustion/incineration [4–6]. New generations are pushing the legislation towards environmental consciousness, forcing the industry to adopt more recycled products in their manufacturing process [1,7]. Our research project aims at developing new composite

materials made out of recycled carbon black from waste tires by an eco-friendly vacuum pyrolysis process [2,8].

Waste tire pyrolysis (see Figure 1) is a process of thermal decomposition of organic materials under heat in a controlled non-oxidative condition, leading to three main sub-products: a solid residue, and gaseous or liquid hydrocarbons. The hydrocarbon sub-products can be revalorized, and the solid residue, so-called the char, can be retreated for its valorization. The pyrolysis char is mainly composed of carbon black and other organic solid materials contained in the tire composition [8,9]. Carbon black (CB) is a common filler used to provide UV protection to polyolefin plastic applications, such as piping, roof membranes, electric cables and wires, geotextiles, and other outdoor products [10–12]. Commercial carbon black is made by thermal decomposition or partial combustion of hydrocarbons such as oil or natural gas. The tire industry is a major end user of carbon black particles. In the USA, the tire industry is responsible for 70% of the total production of carbon black [13]. Commercial CB, typically used in composite materials manufacturing, generates a carbon footprint of 1.08 kg CO<sup>2</sup>/kg of CB (ecoinvent v3.6 database [14]). The substitution of newly produced CB by rCB from waste tire pyrolysis reduced the carbon footprint to 0.43 kg CO<sup>2</sup>/kg CB [14]. The pyrolysis recycling of CB therefore makes it possible to reduce carbon footprint by 60% while being at a competitive price.

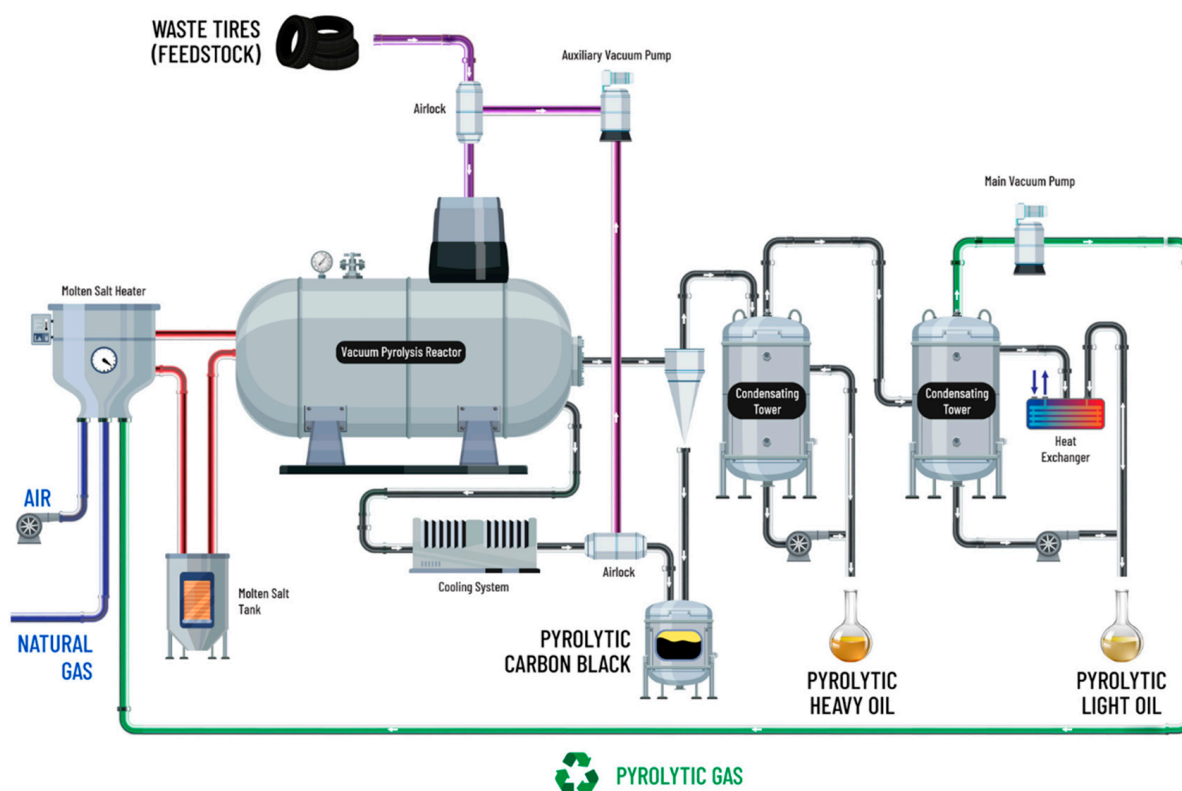


**Figure 1.** Vacuum pyrolysis process of Pyrovac Inc.

Furthermore, the commercial value of the recycled carbon black is increasing as recycling processes are being developed and optimized to produce good-quality particles at high rates. The ability to replace commercial carbon black by recycled solutions is directly related to the capability of the pyrolysis process of waste tires [3,15]. The quality and consistency of pyrolytic recycled carbon black can vary significantly, in particular because it contains various different carbon black grades used in the tire composition and because of the diversity of tires in the recycling process (from cars, trucks, tractors, bikes, etc.). This high variability of mixed tires and particles makes it difficult to optimize the pyrolysis processing conditions to aim at recovering a certain grade of carbon black

particles for a specific use [16]. In addition, the pyrolytic carbon black contains a portion of ash (12–17 wt.%) and carbonaceous deposits on the surface of the particles [9,17], making the particles smoother. These deposits have a detrimental impact on the surface area of the particles and on their ability to bond, and therefore reduce their performance in reinforcing plastics and elastomers [18,19]. Carbonaceous deposits are the result of thermal cracking due to an accumulation of volatiles during tire decomposition, which has the effect of clogging the pores of the particle. The vacuum pyrolysis process of Pyrovac Inc. makes it possible to limit these side reactions because the volatiles hydrocarbons are constantly evacuated by the vacuum pressure [9]. Pyrolytic carbon black thus has surface properties that are closer to those of commercial carbon black used in the composition of tires [18]. The recycling process of waste tires is crucial from an ecological perspective but also presents new avenues for industrial utilization of the recovered materials [20].

Plastic materials exposed to direct sunlight radiation conditions, such as in tropical climates, require tailored UV protection and anti-oxidant capability for long-term durability. Typical sunlight radiation in tropical areas is characterized by high temperatures (annual average of +26 °C), high relative humidity (annual average of 70–80%), and solar irradiation of more than 200 KWh/m<sup>2</sup> [21,22]. These environmental conditions are the primary cause of polymer degradation, having a significant impact on their durability [21]. Polyolefins are the most used polymers in industry and are sensitive to UV radiation and temperature, which affects their mechanical performance over time. The degradation mechanism of polyolefins has been extensively studied by researchers [22–25]. It starts with a photolysis reaction of one of the chromophores present in the polymer, leading to the formation of free radicals that react with the polymer chains in the presence of oxygen. Oxidation products are then formed according to a loop mechanism [22,26]. Chemical aging affects the molecular structure of the polymer, mainly with chain scissions and crosslinking, having an impact on mechanical properties and on the surface aesthetic of the polymer (discoloration). To improve their durability, a typical approach consists in mixing the polymer with solid particles to act as a filter for sun rays. Carbon black is a material known for its sun radiation absorption performance; it acts as a radical scavenger, a radical trap, or a UV absorber [11,12,27,28]. It should be noted, however, that it can also have the opposite effect, acting as a pro-oxidant, as reported by Horrocks et al. for polypropylene composite tapes made with carbon black [12]. This would be due to the concentration of oxygenated groups on the surface of the carbon black particles, which would adsorb the antioxidants present in the polymer or by thermo-oxidative reactions on the surface of the particles, the carbon black acting as a catalyst in the peroxide decomposition and the formation of the free radicals, enhancing the oxidation process. The surface of carbon black particles has to be treated to reduce oxygenated groups and to grasp functional groups for better adhesion to the polymer.

Recovering CB from waste tires is challenging due to the impurities in the particles, where many different processes have been studied to improve the surface quality of the rCB [29]. In this study, the vacuum pyrolytic rCB has the benefit of a clean surface as the vacuum helps extract the impurities as these are pulled out by the evaporating gases in the chamber. The resulting rCB is cleaner and oxidized at the exit of the pyrolytic chamber to improve its affinity with the polymer [30]. While the original vacuum pyrolysis process presented above was used to recover CB from waste tires, it did not devise the use of the oxidative functionalization as presented in this research, and no composites were made at the time. The functionalization of CB and post-pyrolysis processes to produce the HDPE-rCB composite presented in this research is new to the authors.

In this work, the recycled carbon black (rCB) from vacuum pyrolysis of waste tires was used as UV protection filler in a high-density polyethylene (HDPE) matrix. To study the protection performance of recycled carbon black, HDPE samples with and without recycled carbon black were aged under accelerated conditions. FTIR spectroscopy was used to detect the change in sample oxidation over time, and the surface topography of the samples was studied by optical microscopy. The amount of oxidation products as a

function of the sample thickness was also evaluated on pure HDPE and HDPE containing rCB. The depth oxidation distribution profiles were fitted using a Beer–Lambert law. The antioxidant action of the recycled carbon black is finally discussed.

## 2. Materials and Methods

### 2.1. Materials

The recycled carbon black (rCB) used is supplied by Pyrovac Inc. It was obtained by vacuum pyrolysis (530 °C, 15–20 kPa) of waste tires and comes from a demonstration industrial plant of 540 kg/h located at Ville de Saguenay (Québec, Canada) and has received no post-treatment. The tire recycling process is reported in Roy et al. [9]. The rCB used in this work [9] has a surface area of 77.3 m<sup>2</sup>/g (multipoint nitrogen surface area), a structure of 95 cm<sup>3</sup>/100 g (oil absorption number), and an ash content of 15.7 wt.% [9].

High-density polyethylene from Dow Chemicals (HDPE Dow<sup>TM</sup> DMDA-8904 NT 7) was used in this study as the plastic resin. This material is largely used in outdoor plastic applications, and in particular in piping, which allows a possible application for the irrigation of crops in the agricultural field in tropical climates, such as Guadeloupe. It has a melt index of 4.4 g/10 min and a density at room temperature of 0.952 kg/m<sup>3</sup> [31]. The choice of using a petroleum (and non-recycled) HDPE matrix was made in order to limit the only variability related to recycling to the carbon black particles.

This research only focuses on rCB/HDPE composites, while previous studies were more generalized in the study and comparison of rCB composites with commercially available CB [32,33].

### 2.2. Sample Preparation

Figure 2 shows the steps carried out in this work during the preparation of the HDPE/rCB composite materials. The average size of rCB particles at the exit of the pyrolysis oven was measured to be around 380 microns in diameter, with a large variability due to the nature of the process and diversity of waste tires. The origin of these large agglomerates is mainly the carbonaceous deposits during the pyrolysis decomposition process. To reduce their size, rCB powder was grinded using a Spex/Mixer Mill 8000M with zirconium oxide beads (step A on Figure 2). Gridding duration was 1 h 30 min in total, with 3 intervals of 30 min. A 10 min water bath cooling of the container was added between each interval.

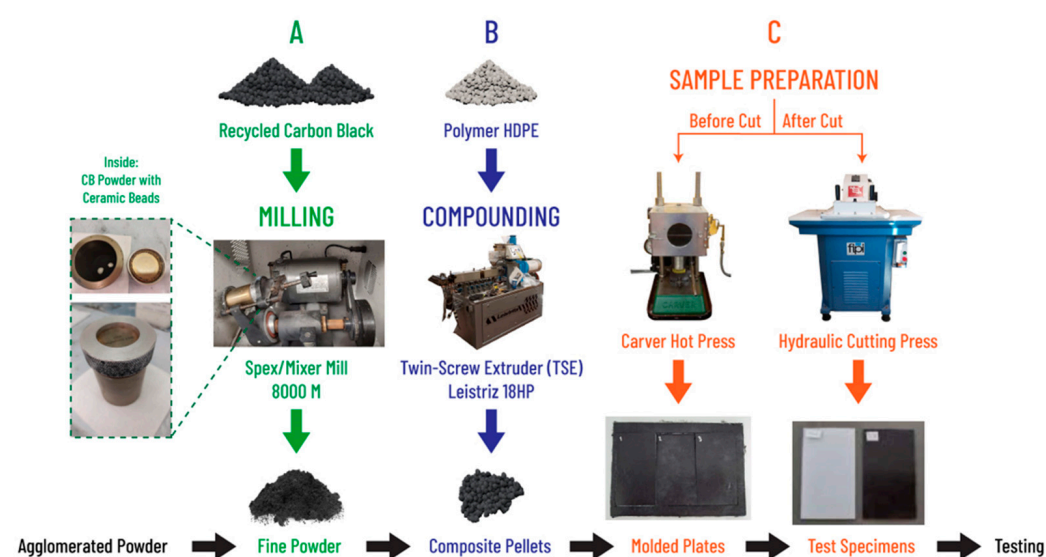


**Figure 2.** Processing steps for the preparation of composites test specimens.

After milling rCB, the composite material was prepared by mixing the melted polymer with carbon black particles using a twin-screw extruder (step B on Figure 2). A Leistritz

18HP twin-screw extruder (TSE) with 8 temperature zones was used with optimized processing conditions for HDPE (see Figure 3). HDPE pellets and 6 wt.% of milled rCB were compounded at a temperature varying from 180 to 200 °C. Since the virgin HDPE pellets already contain a thermal stabilizer, no additional antioxidant was added to the mix. The extruded filament was pelletized at the exit of the TSE to an average size of 3 mm. To have the same thermal history, the unreinforced HDPE was also prepared using the same processing conditions in the TSE as the composite samples. The manufactured samples are named HDPE for the virgin polymer and R6 for the composite containing 6 wt.% of rCB, respectively. The 6 wt.% content was obtained following a test screening of various percentages, and it represents typical values for the industry [32,33].

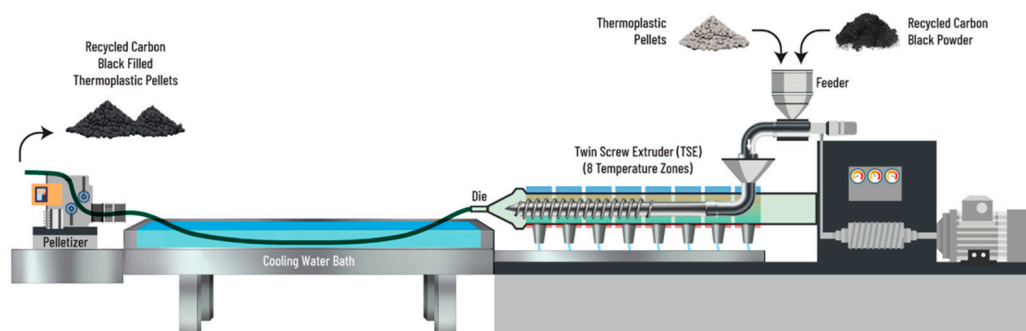


**Figure 3.** Mixing and extrusion of HDPE/rCB composites with a twin-screw extruder Leistritz 18HP.

Polymer and composite pellets manufactured by TSE were molded into plates of 2 mm thickness using a compression molding technique (step C on Figure 2) in a heated hydraulic press (Figure 4). A Carver press with plates heated at 170 °C and a closing mass of 2500 kg was used to press mold rectangular flat plates. The molded plates were then cut in 9 cm per 5 cm test specimens using a hydraulic press and a die cut (step C on Figure 2). These samples were used for the accelerated aging experiments in this study.

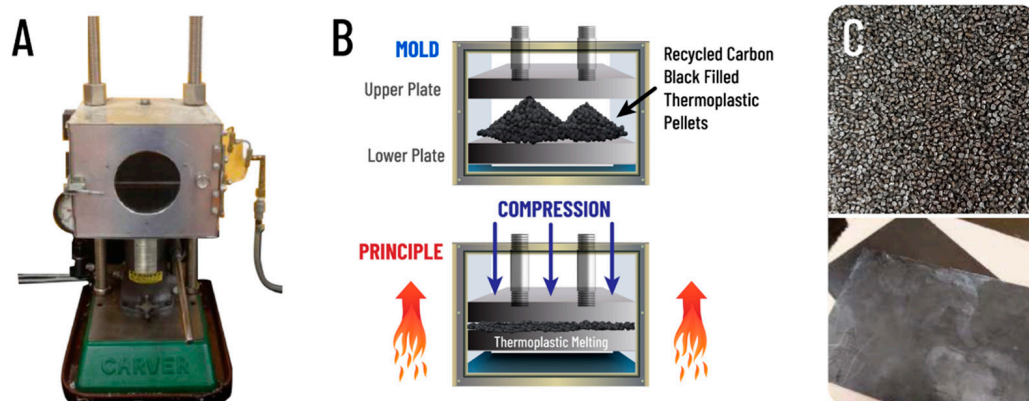


**Figure 4.** Plate molding: (A) Carver hot press, (B) mold and molding principle, and (C) frame containing composite pellets and molded plates.

### 2.3. Sample Aging

Accelerated aging was carried out in a weathering chamber ARTACC from SEVAR. The samples were placed on the outer part of the moving wheel as illustrated in Figure 5. This chamber was built according to the ISO 4892-1 standard. The test specimens were held in place with clips and their internal faces were exposed to a 400 W medium-pressure mercury vapor lamp with an irradiation of 120 W/cm<sup>2</sup> UVA and 20 W/cm<sup>2</sup> UVB (EN 60 188 standard requirements). The temperature inside the chamber was 60 ± 0.1 °C and water was added in the chamber to simulate natural conditions. The samples underwent six cycles per 24 h, alternating between dry and wet cycles, which corresponds to 80% of dry irradiation, 5%

of wet irradiation, and 15% of wet, non-irradiated phases. For the non-irradiated phase, samples were hidden from the UV lamp by a mask (Figure 5). The exposed face of the sample to UV light was named Fe and the non-exposed face Fne (Figure 5).

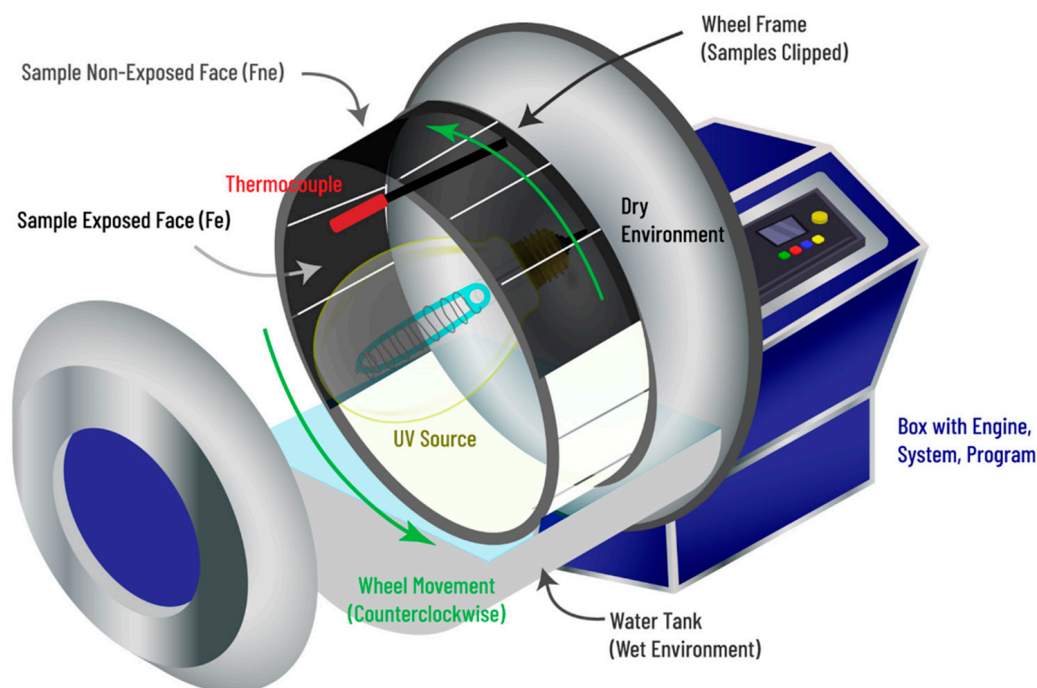


**Figure 5.** Artacc Bandol Wheel diagram with overview of samples placement indicating exposed and non-exposed faces.

#### 2.4. Sample Analyses

The particle size volume repartition of the recycled carbon black was measured using laser diffraction with a Coulter LS analyzer according to the ASTM B822-20 standard. The morphology of the recycled carbon black particles was visualized by high resolution transmission microscopy (HR-TEM) using the JEM-21000F/HR 200 kV from JEOL. Energy dispersive X-ray spectroscopy (EDS-X) was performed on the milled particles to verify their composition using a field emission environmental scanning electron microscope (FEI Quanta 250 FEG-ESEM).

The topography of the surface of the polymer and composite plate samples was studied using a Zeiss Axioskop 2 optical microscope. Particular attention was paid to the occurrence of cracks during aging. For this purpose, a computer program was developed using Python software that made it possible to quantify the surface changes during aging. Image analysis was performed based on grayscale differences and 3 measurements were carried out per face in order to have an overall representation of the sample.

Chemical degradation of the samples and track of the oxidation products was monitored using a Fourier transformed infrared spectroscopy (FTIR) [22,25,34] with a Perkin Elmer Spectrum Two spectrometer. The FTIR measurements were performed in the attenuated total reflectance (ATR) mode, with a range of 500–4000  $\text{cm}^{-1}$  wave numbers and a resolution of 4  $\text{cm}^{-1}$ . To improve the signal, each spectrum corresponds to 64 accumulations. The FTIR measurements were performed on the exposed and the non-exposed faces with 3 measurements per face to study the homogeneity of the surface oxidation. In all cases, to avoid having edge effects, the measurements were taken more than 10 mm from the edges of the plates. The absorption ATR spectra were processed using OriginPro 2020 (v9.7) from OriginLab analysis software.

For the through-thickness oxidation profiles, the samples were gradually polished using 1000 grade sandpaper. FTIR measurements were performed at each decrease in thickness and were associated with the new thickness resulting from polishing. The

polishing was carried out from both the Fe and Fne faces. The material removal was measured using optical microscopy and measurement tools of the microscope software.

### 3. Results and Discussion

#### 3.1. Carbon Black Analyses

The average diameter of rCB particles from pyrolysis is too large to be directly processed into a thermoplastic resin. Large agglomerates >500 microns are observed and most probably linked to residual carbonaceous deposits from the process, which promote the agglomeration of the particles. Carbonaceous deposits are the result of thermal cracking in the pyrolysis oven; they are hard as they contain a high amount of carbon, and shear forces generated during the extrusion process are not sufficient to deagglomerate the particles. A secondary upstream process is needed to reduce the size of the agglomerates before they can be incorporated into the polymer resin. Size reduction was carried out using a ball mixer with zirconium oxide balls in dry conditions. Figure 6 illustrates the volumetric ratio of the powder distribution of the rCB before and after milling and the cumulative percentage. A shift in the average particle size toward lower sizes is observed at more than 1 order of magnitude. The mean size of the agglomerates is reduced by 94% from 380 to 20 microns. The milled rCB also shows more than 20% of particles with a size of less than 10 microns, which is expected to improve the mechanical performance of the composite.

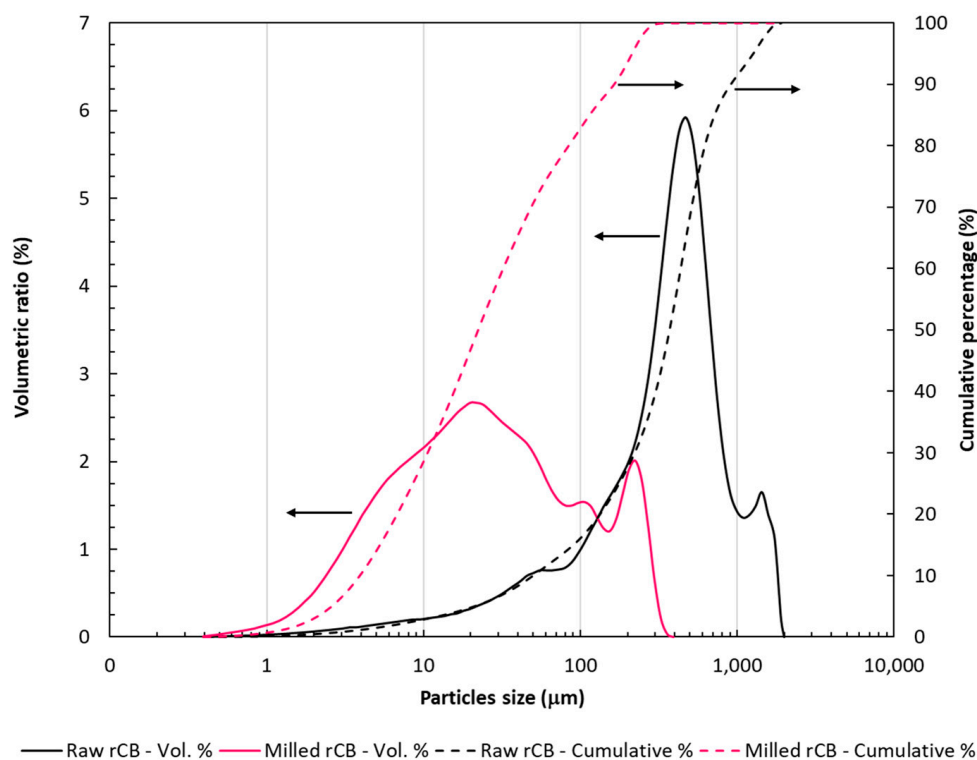


**Figure 6.** Volumetric ratio of powder distribution (line) and cumulative percentage (dash) of recycled carbon black (rCB) before (black) and after (red) ball milling.

Energy dispersive X-ray spectroscopy (EDS-X) analyses were performed on rCB particles (Figure 7) to verify the composition of the particles and whether they may have been contaminated by the zirconium oxide beads. The rCB shows that it contains mainly elemental carbon, oxygen, and the remaining solid residues from the pyrolysis process that enter the original waste tire composition. The solid additives based on the total remaining residues (removing oxygen and carbon) contain an atomic percentage of  $27 \pm 3\%$  for silicon,  $35 \pm 1\%$  for sulfur,  $31 \pm 3\%$  for zinc, and  $6 \pm 1\%$  for calcium. The EDS-X analysis reveals no significant contamination by the zirconium oxide  $ZrO_2(Y_2O_3)$  ceramic beads

during the milling process. Thus, grinding should not make any changes other than size reduction of the agglomerates.

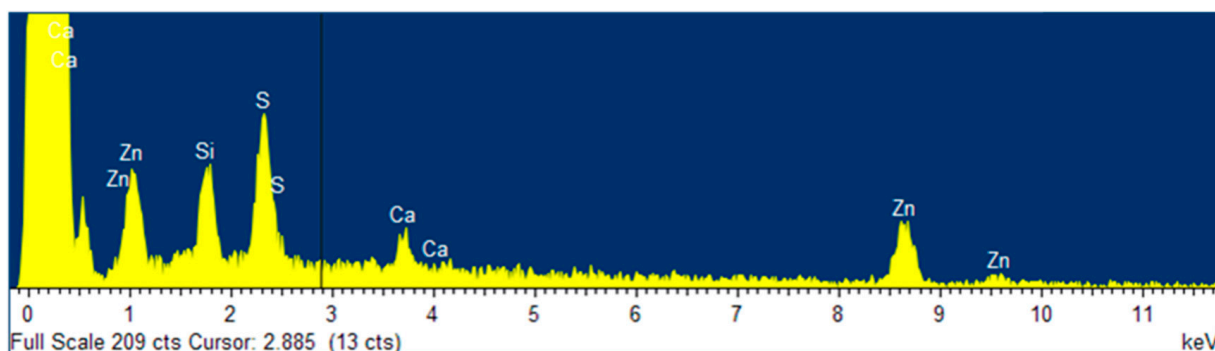


**Figure 7.** Typical spectrum ESEM EDS-X analysis on rCB particulates.

An additional verification was carried out for the morphology of the carbon black particles. This has been investigated using HR-TEM, as illustrated in Figure 8. The milled rCB particles (Figure 8b) were compared to a typical commercial carbon black grade used for automotive tire tread, the ASTM N330 (Figure 8a). As illustrated, the two types of particles are very similar, both showing stacked graphitic layers in concentric circles, a structure typical of carbon black [35–38].

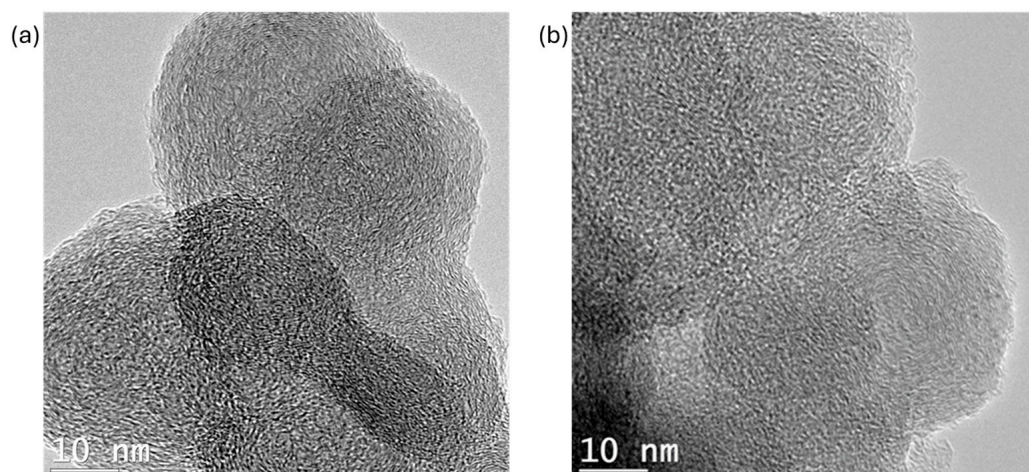


**Figure 8.** HR-TEM image: (a) N330 commercial carbon black used for automotive tire treads, and (b) recycled carbon black.

### 3.2. Evolution of Sample Topography with Aging

The virgin polymer resin HDPE and the composite R6 samples were taken periodically out of the aging chamber, and their surface appearance was observed by optical microscopy. Figures 9 and 10 show the optical micrographs recorded, respectively, on HDPE- and R6-exposed and non-exposed surfaces at different aging times, up to 114 days. The non-exposed (Fne) and exposed (Fe) faces are presented in the left and right columns, respectively, for comparison.

The virgin HDPE (Figure 9) shows that the exposed face starts to crack at 22 days, whereas the non-exposed face shows cracks at 36 days of aging. The cracks on Fe at 36 days of aging appear much larger than on Fne. At 64 days, the network of cracks is largely visible and even worse after 114 days of UV exposure. Similar observations were made for polypropylene–polyethylene copolymers exposed to UV accelerated aging conditions in a study by Pertin [39]. Crack propagation is indeed the dominant mechanism of polymer degradation under UV radiation [40,41].



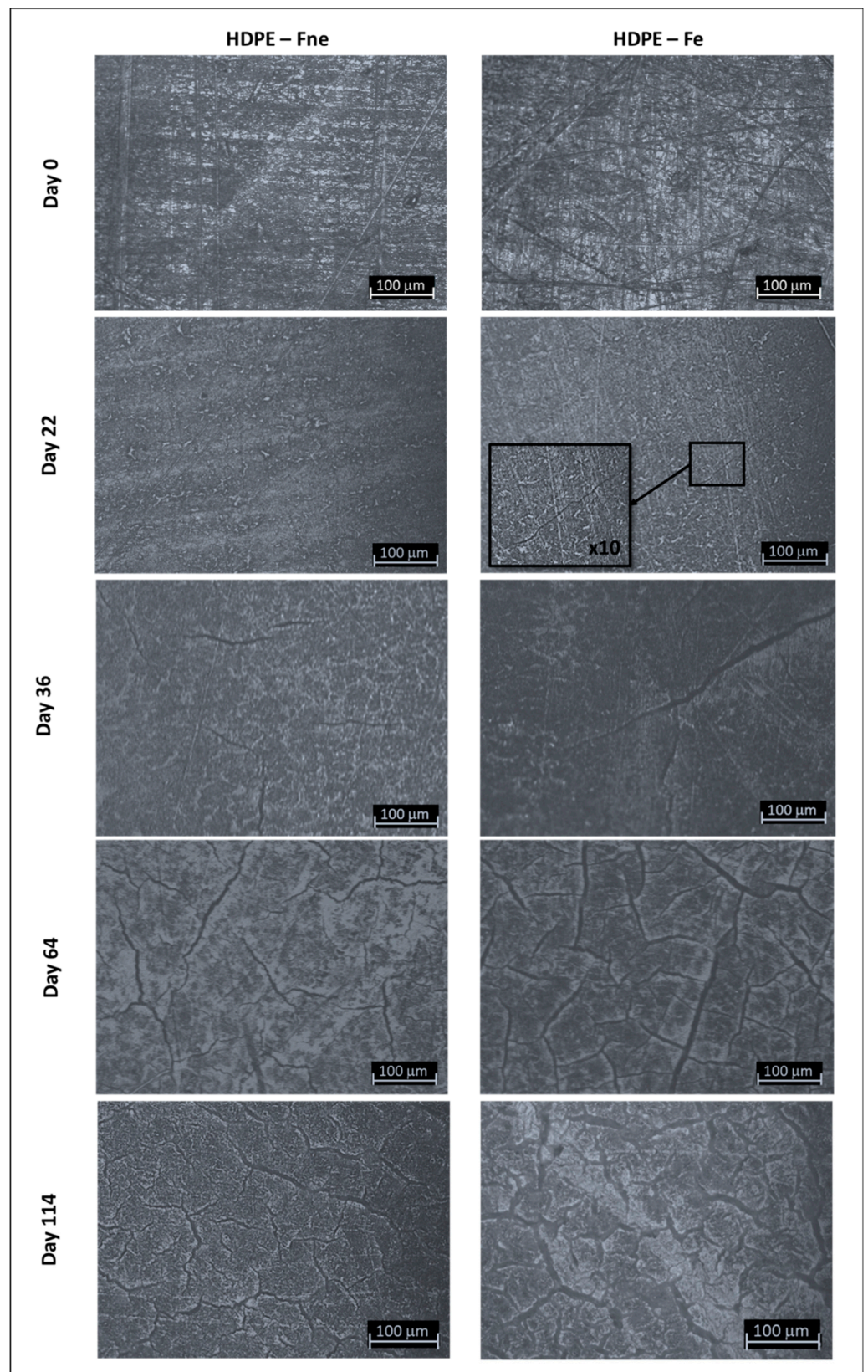
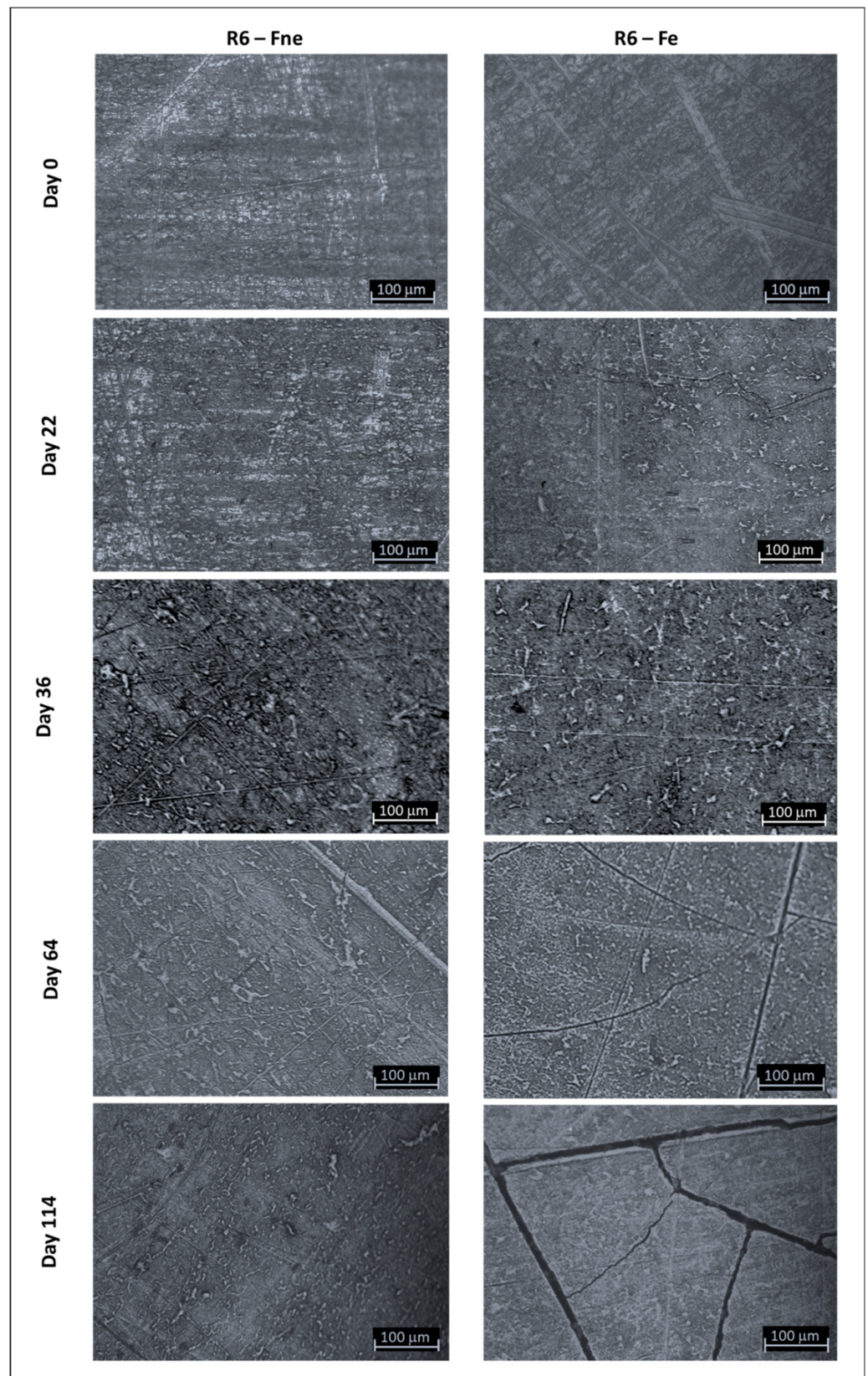


Figure 9. Optical microscopy images of HDPE samples at different aging times.



**Figure 10.** Optical microscopy images of R6 samples at different aging times.

The HDPE/rCB samples R6 show the non-exposed face Fne remains unchanged over time with no signs of cracks, even at 114 days of aging, as illustrated in Figure 10. For the R6-exposed face Fe, cracks start to appear after 64 days of UV exposure and are largely

visible after 114 days. Furthermore, cracks do not propagate in the R6 composite the same way they do in virgin HDPE: in HDPE, cracking is significantly important, resulting in macro cracks propagating into micro cracks, which is not the case for R6, where only macro cracks are observed on the surface. This highlights the role of carbon black in filtering UV and consequently reducing polymer degradation and crack propagation.

In order to quantify the crack density, image analysis was carried out using Python software. Figure 11 illustrates the evolution of the surface percentage of cracks during aging for HDPE and R6 samples. Each surface ratio is the average of three representative images, and the error bars are the associated standard deviation. Hence, the calculation considers the differences in surface homogeneity. The results confirm the microscopy observations. For HDPE, the surface ratio of cracks evolution with aging time is similar for both Fe and Fne surfaces, the crack density being slightly higher on the exposed face. From 30 days of aging, the crack ratio increases almost linearly with time, reaching 20% at 114 days of UV exposition for the Fe surface. Such a percentage reflects a strong degradation of the surface of the sample. For the Fne surface, the same trend is observed with a slightly lower percentage of cracking, which reaches a value of 13% at 114 days of aging. For R6-Fe, the surface ratio of cracking is significantly lower, not exceeding 5% at 114 days of aging.

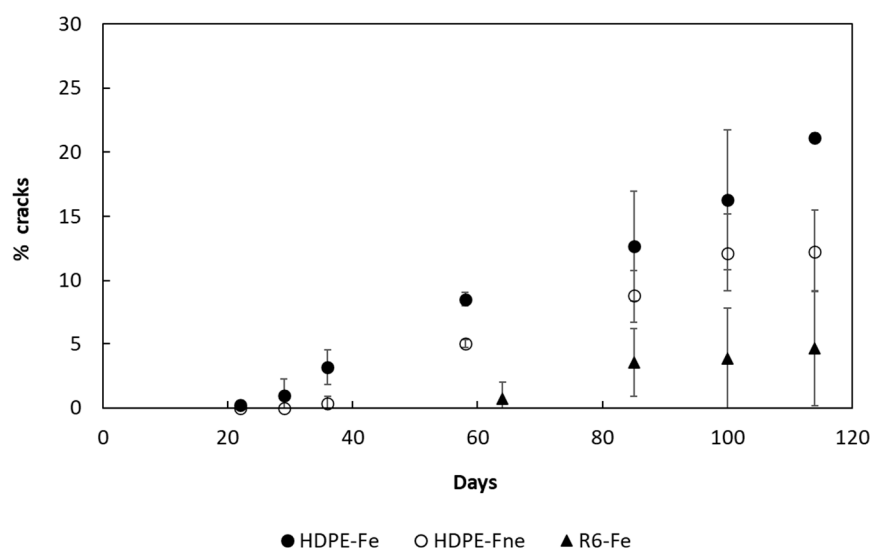


**Figure 11.** Evolution of the average surface percentage of cracks during photooxidation for HDPE and R6.

The standard deviation of the measurements reflects the inhomogeneity of the surfaces of the aged samples. For HDPE-Fe, this standard deviation is low at the beginning because the surface only starts to weakly crack, evenly on the plate. Thereafter, it becomes important because the cracking develops mainly in the center of the plate. At 114 days of aging, the surface is completely covered with cracks, which results in a low standard deviation. This is not the case for the Fne side, which is not yet totally degraded. In the case of R6-Fe, the appearance of cracks remains inhomogeneous and concentrated in the center of the sample, which results in a significant standard deviation.

The apparition of cracks is probably due to a gradient of elasticity in the sample thickness, which is shown by a variation in the Young's modulus value as reported by Pertin et al. [42]. During artificial aging, samples undergo thermal expansion, and mechanical stresses are buildup on the UV-exposed layer and probably released by the occurrence of cracks [42–44].

### 3.3. Degradation Kinetic and Formation of Oxidative Products

A typical FTIR spectrum of an 85-day-aged HDPE is shown in Figure 12a. Three main regions are connected to the oxidation process: the C=C bands ( $700\text{ cm}^{-1}$  to  $1300\text{ cm}^{-1}$ );

the C=O bands ( $1500\text{ cm}^{-1}$  to  $1850\text{ cm}^{-1}$ ); and the O-H bands ( $3200\text{ cm}^{-1}$  to  $3600\text{ cm}^{-1}$ ). Table 1 summarizes the FTIR absorption spectrum of the HDPE and its main oxidation products usually reported in literature [25,34,45–48]. In this work we have focused on the C=O band region only, which is the band where the oxidation first appears in HDPE [25,34] and remains predominant in this work. An enlarged view of the carbonyl oxidized region between  $1500\text{--}1850\text{ cm}^{-1}$  wavelength is illustrated in Figure 12b. The band deconvolution shows three main peaks: carboxylic acid/ketone around  $1715\text{ cm}^{-1}$ ,  $\gamma$ -lactone at  $1780\text{ cm}^{-1}$  and vinyl at  $1640\text{ cm}^{-1}$ . These peaks are characteristic of HDPE polymer oxidation products, and the cumulative band (red curve) fits well with the experimental data (black curve). The carbonyl region is the most apparent for both the virgin HDPE and composite R6, and more specifically the band C=O at  $1715\text{ cm}^{-1}$ . The other absorption bands are less well defined, especially for R6, where they are sometimes even confused in the baseline. The baseline indeed presents variations in absorbance of 0.0076 unity of absorbance (u.a.) in the initial FTIR spectra of both HDPE and R6 inside the carbonyl region ( $1500\text{--}1850\text{ cm}^{-1}$ ). Absorbance bands below this value are therefore considered as signal noise. Oxidation was quantitatively analyzed using the carbonyl index (CI) using the SAUB method [49] and defined as follows:

$$CI = \frac{\text{Area under band at } 1715\text{ cm}^{-1}}{\text{Area under band at } 2912\text{ cm}^{-1}} \quad (1)$$

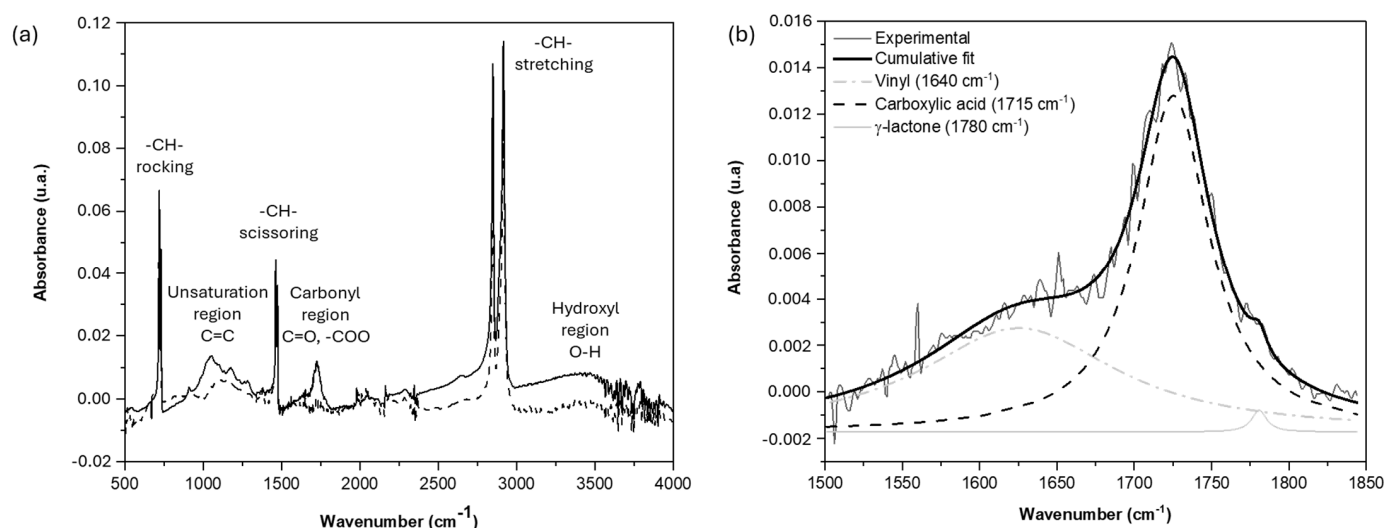


**Figure 12.** IR spectra of weathered HDPE sample at 85 days: (a) global experimental curve of aged (black line) and non-aged (black dash) samples and (b) zoom on the carbonyl region of the aged sample and peak deconvolution. Experimental curve (black line); cumulative fit (thick black line); vinyl (gray dash dot); carboxylic acid/ketone (black dash);  $\gamma$ -lactone (gray line).

**Table 1.** Spectral FTIR bands studied for HDPE.

Wavenumber [ $\text{cm}^{-1}$ ]	Functional Groups	
HDPE Initial Bands		
720	C-H rocking, amorphous	$\text{CH}_2$
730	C-H rocking, crystalline	$\text{CH}_2$
1464	C-H scissoring, amorphous	$\text{CH}_2$
1474	C-H scissoring, crystalline	$\text{CH}_2$
2846	symmetric C-H stretching	$\text{CH}_2$
2912	assymmetric C-H stretching	$\text{CH}_2$

Table 1. Cont.

Wavenumber [ $\text{cm}^{-1}$ ]	Functional Groups	
Unsaturation Region		
888	Vinylidene	$\text{CH}_2=\text{CR}_2$
909	Vinyl ( $\text{C}=\text{C}-\text{H}$ out of plane bending)	$\text{CH}_2=\text{CHR}$
965	Vinylene ( $\text{C}=\text{C}-\text{H}$ bending)	(Trans) $\text{R}-\text{CH}=\text{CH}-\text{R}'$
Carbonyl Region		
1640	Vinyl ( $\text{C}=\text{C}$ vibration)	$\text{C}=\text{C}$
1695	Conjugated ketone	$\text{CH}_2=\text{CH}-\text{CO}-\text{CH}_3$
1715	Carboxylic acid	$\text{R}-\text{COO}$
1720	Ketone	$\text{R}-\text{C}=\text{O}-\text{R}'$
1740	Ester	$\text{R}-\text{COO}-\text{CH}_2$
1760	Peracid	$\text{R}-\text{COO}-\text{OH}$
1780	g-Lactone	$(\text{CR}_2)_n\text{CO}-\text{O}$
Hydroxyl Region		
3400	Hydroperoxide + alcohol groups	$\text{R}-\text{COOH}-\text{R}$

This defines the ratio between the area under the absorbance of  $\text{C}=\text{O}$  at  $1715 \text{ cm}^{-1}$  and the area of the methylene stretching peak at  $2912 \text{ cm}^{-1}$ . The latter was chosen as the reference band because it is not altered during aging [45]. To avoid IR absorption variations due to the presence of CB in the composite, a reference FTIR spectrum is obtained for each individual sample to calculate the aged *CI* index. This method eliminates the initial signal noise that may occur due to the presence of CB in the samples. Details of the reference *CI* calculation can be found in [33].

Figure 13 illustrates the evolution of *CI* of virgin HDPE (Figure 13a) and composite R6 (Figure 13b) of the exposed face (plain symbol) and non-exposed face (open symbol) for a maximum aging time of 114 days. The *CI* was calculated using Equation (1). The data shown are the results of the average of three measurements for each of the faces, and the error bars represent the associated standard deviation. The evolution of the *CI* of Fe and Fne of HDPE is very similar (Figure 13a). Initially, the *CI* values of Fe and Fne overlap below 20 days, then differ slightly. The *CI* of the Fe faces start to be higher than that of the Fne faces after 30 days of aging, although the differences are very close to the error bars. The induction period is less than 10 days, and the *CI* reaches a saturation plateau value of 30 after 60 days of exposure on both faces. Since ATR analysis is a surface measurement, the saturation observed indicates that the surface layers analyzed are fully oxidized.

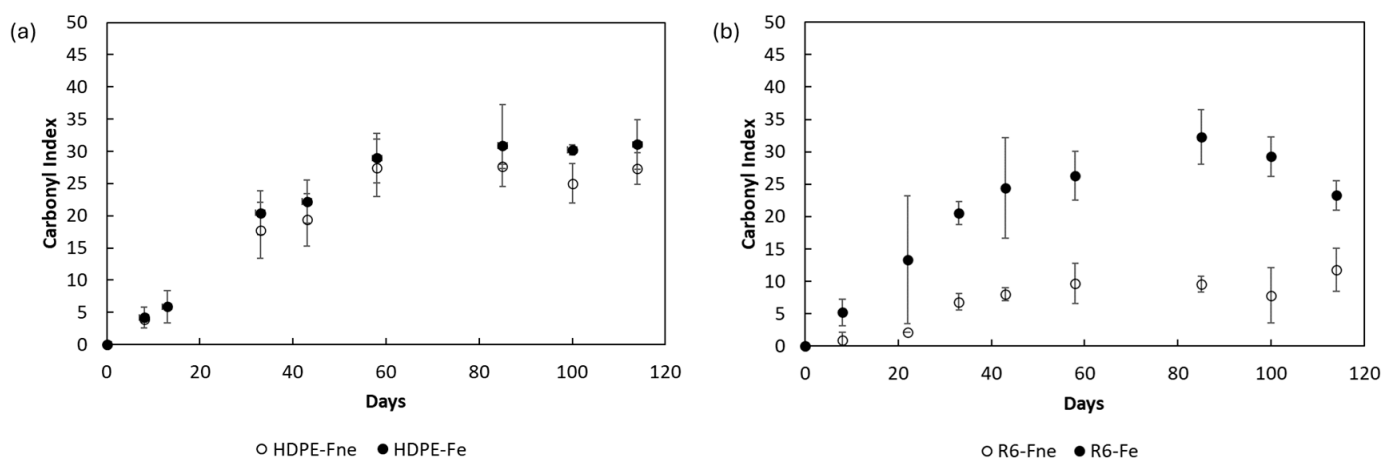


Figure 13. Evolution of the carbonyl index with aging time for (a) HDPE (b) R6. Open symbols are for the non-exposed face and plain symbols are for the exposed face.

*CI* measured on the Fe faces of R6 samples shows similar behavior than that of the HDPE Fe faces, as illustrated in Figure 13b. The induction period is less than 10 days, and

a *CI* maximum value of 30 occurs at 60 days. Up to 100 days of aging, the *CI* values are identical to those measured on the Fe face of HDPE, considering the error bars. A slight decrease is observed for aging times greater than 100 days, as a *CI* value of 24 is measured at 114 days of aging. The reason for this small *CI* reduction value is under investigation. The quasi-identical results obtained on the Fe face of HDPE and R6 samples indicated no significant influence of the rCB particles on the oxidation process of the UV-exposed faces. On the other hand, a quite different behavior is observed for the Fne face of R6 samples. The induction period is longer, close to 20 days (instead of 10 days), and the *CI* values are significantly lower than those on the Fe face. The saturation value is below 10. This result clearly indicates that the recycled carbon black plays a key role in the antioxidant process for the bulk.

To investigate the oxidation beyond the surface, analyses were carried out on the thickness of the HDPE and the R6 composite samples. For this purpose, the samples were gradually polished and measured for each thickness in FTIR spectroscopy. The *CI* was calculated using Equation (1). Figure 14 presents the evolution of carbonyl concentration through the thickness of HDPE and R6 at 114 days of aging. The surface directly exposed to UV light, Fe, is referenced at a 0 mm depth, and the non-exposed surface, Fne, is referenced at a 2 mm depth. The oxidation profiles measured on both samples are U-type curves, as already observed for thick polyethylene [23] and polyolefins [39,40]. The experimental data of the oxidation profiles have been fitted using an exponential curve of the Beer–Lambert law as already reported in other works [42,50]. The following formula was used:

$$CI(x) = A \exp(-x/B) \quad (2)$$

where  $x$  is the sample thickness,  $A$  is the *CI* value at the surface, and  $B$  is the characteristic depth of the oxidation profile. The corresponding fitting curves are shown in Figure 14, with the blue curve for HDPE and the red one for R6. The values of  $A$  and  $B$  calculated for the Fe and Fne faces of HDPE and R6 samples are reported in Table 2. The HDPE curves are quasi-symmetrical for Fe and Fne, and the characteristic depths of oxidation are similar ( $162 \pm 33 \mu\text{m}$  for Fe compared to  $146 \pm 19 \mu\text{m}$  for Fne).

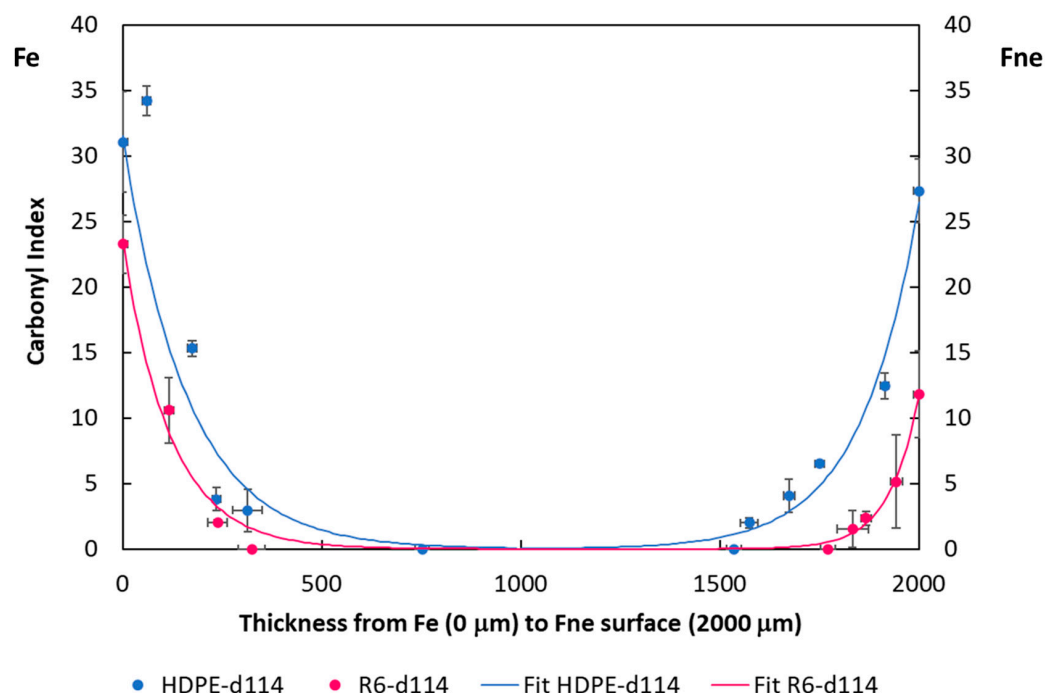


**Figure 14.** Evolution of the carbonyl concentration through thickness from the exposed face (Fe) to the non-exposed face (Fne).

**Table 2.** Parameters of the carbonyl index distribution with the thickness for HDPE and R6 at 114 days of aging using an exponential fit.

Material	Face	Coefficient	Value		R <sup>2</sup>
HDPE	Fe	A	32 ± 3	mm	0.926
		B	162 ± 34		
HDPE	Fne	A	26 ± 2	mm	0.971
		B	147 ± 19		
R6	Fe	A	24 ± 2	mm	0.970
		B	120 ± 20		
R6	Fne	A	11.7 ± 0.4	mm	0.990
		B	74 ± 6		

For the R6 sample, the Fne and Fe profiles are asymmetric; the *CI* measured for the non-exposed face Fne is 50% lower than that of the Fe face. The depth of the oxide layer close to the Fne-R6 face is also significantly smaller ( $B = 74 \pm 6 \mu\text{m}$ ) compared to the Fe-R6 face ( $B = 120 \pm 20 \mu\text{m}$ ). Note that the A and B profile parameters for Fe-R6 are quite similar to those measured on the Fe-HDPE sample, although slightly lower. These results highlight that the carbon black particles issued from tire recycling do not have prooxidative action and that, on the contrary, have a totally opposite behavior and act like an antioxidant.

It is well known that the oxidation process is associated with two combined mechanisms: the formation of free radicals induced by UV absorption and the presence of oxygen [41,47]. The quasi-symmetric profile observed for HDPE clearly indicates that the photon flux passes through the sample without being significantly absorbed: the quantity of photons being identical on both faces and so the supply of oxygen; the oxidation process is similar. The decrease of *CI* value with depth observed for HDPE samples is clearly related to the non-ability of oxygen to diffuse into the bulk of the polymer [23,51]. Figure 15a schematically summarizes the symmetric oxygen diffusion profile (black curve), the photon propagation profile (blue dashed line), and the resulting *CI* profile (blue line) for HDPE.

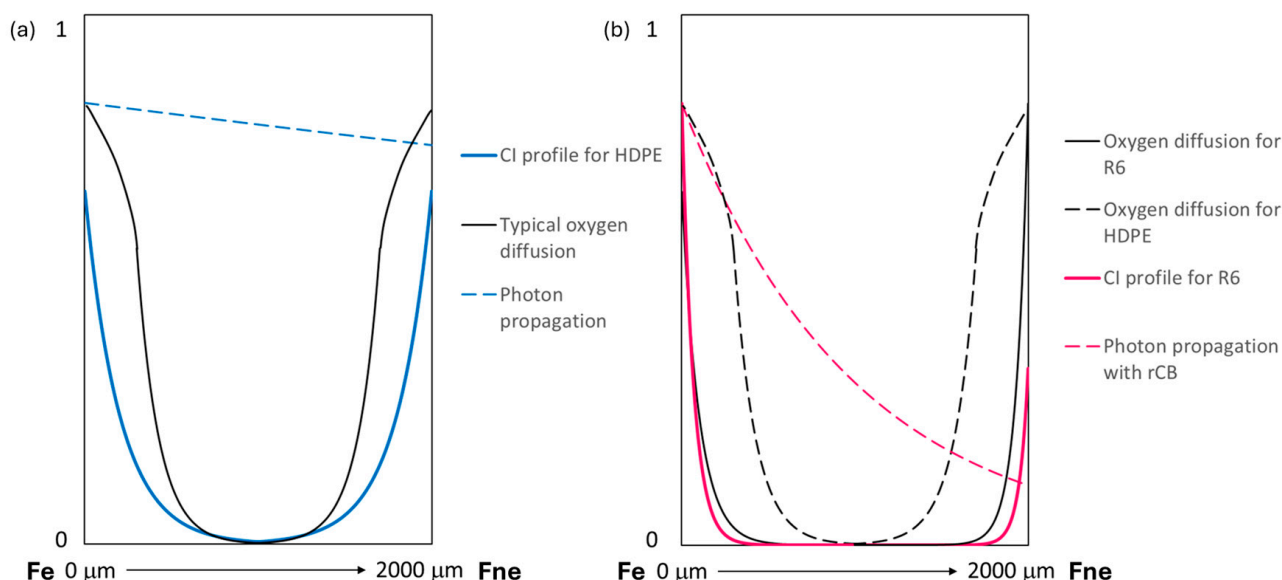


**Figure 15.** Diagram of the evolution of the oxygen diffusion and the photon propagation and *CI* through thickness for (a) virgin HDPE and (b) R6 composite.

Since the oxygen supply is identical for both Fe and Fne faces of the sample, the lower carbonyl index measured on the surface of R6-Fne is clearly related to a lower flux of photons reaching the Fne face due to UV absorption through the thickness of the R6

sample (red dashed line reported in Figure 15b). This result confirms the role of rCB as a photon absorber. There is also a significant difference in the characteristic depth of the oxide layer of the Fne and Fe faces ( $11.7 \pm 0.4 \mu\text{m}$  for Fne-R6 and  $24 \pm 2 \mu\text{m}$  for Fe-R6), which suggests that the rCB also affects the diffusion of oxygen into the R6 sample. Also, the surface crack density (see Figure 11) has certainly an influence on the oxidation depth (B parameter). The presence of cracks on the surface of the sample allows the infiltration of the free oxygen, which leads to a higher oxidation depth. This explains the higher B values of Fe-HDPE, Fne-HDPE, and Fe-R6 compared to Fne-R6, where no cracks were observed on the sample surface.

In fact, if the oxygen profile was identical for HDPE and R6 samples (black dashed line in Figure 15b), the characteristic oxidation depths would be expected to be identical since photons pass through the total thickness for both samples. In order to explain the lower characteristic depth observed for R6 samples, we suggest that the oxygen diffusion is also limited by the presence of rCB particles; the carbon black would also act as a radical scavenger, preventing the radical propagation and thus the oxidation process [12,28]. In the first layers close to the surface, the polymer would be weakly protected against photo-oxidation by the addition of the recycled carbon black alone. However, in the deeper layers, the carbon black, which acts as a UV and oxygen filter, becomes more effective as an oxidation protector. The present work clearly demonstrates that the carbon black issued from waste tire pyrolysis is a promising antioxidating agent. The rCB acts as a photon absorber and limits the UV penetration in the composite. A more detailed explanation of the protection mechanism is presented in [32].

#### 4. Conclusions

The general goal of this research is to develop a new composite material using recycled carbon black (rCB) from waste tires to reinforce HDPE. At first, an optimization of the recycled carbon black particles was conducted to deagglomerate the carbonaceous deposits. Grinding of the recycled carbon black particles has allowed them to reduce their size close to the nanoscale, which made it easier to disperse them in the HDPE polymer. Good-quality composite pellets were obtained by the mixing/extrusion process in a twin-screw extruder. The performance of the rCB as a filler for UV protection of HDPE was demonstrated by an accelerated aging test using an ARTACC environmental chamber. Surface topography analysis of the face exposed to UV radiation of the composite R6 has shown much less cracking than the virgin HDPE polymer (cracks appearing 42 days later). HDPE has shown macro- and micro-cracking on both faces (Fe and Fne), whereas for R6 samples the exposed face shows only macro-cracking and the non-exposed face remains unchanged. This highlights the role of rCB in preventing the propagation of cracks in the polymer.

The FTIR results have shown that the rCB added to the polymer has not only an absorption protective action against UV radiation but probably plays a significant role in oxygen diffusion through the sample. The composite R6 shows less surface oxidation (CI 24% less for the Fe surface) than the virgin HDPE, and the photons penetrate less through the sample thickness (CI reduced by 54% for Fne surface). The oxidation profile of the composite is also different between the two surfaces of the exposed and non-exposed faces, as opposed to HDPE, where they are nearly identical. This illustrates the absorption role of rCB, which hinders the penetration of photons. The oxidation in the sample bulk is reduced by more than half for R6 in comparison to HDPE ( $120 \mu\text{m}$  from Fe and  $74 \mu\text{m}$  from Fne, for R6).

This study has demonstrated that the recycled carbon black resulting from waste tire vacuum pyrolysis is a promising approach to revalorize tire waste with an eco-responsible processing. The use of rCB as filler for HDPE used for outdoor applications has demonstrated to be an antioxidant for UV protection and a good substitute for commercial carbon black for industrial goods. In the ecological perspective, the vacuum pyrolysis process used in this study can be easily implantable in limited access areas, such as the Guadeloupe Island, to overcome the ecologically devastating reality of waste tire land fields.



Current studies focus on improving recycled black by surface modifications to improve functionalization, adhesion to the polymer matrix, and reduce aging.

**Author Contributions:** Conceptualization: C.B. Methodology: C.B. Experimental, analysis and validation: C.B. Investigation: C.B. Resources: E.R., L.R., A.F., S.K. Writing—Original draft preparation: C.B. Writing—Review: E.R., L.R., A.F., S.K. Project Administration: E.R., L.R. Supervision: E.R., L.R., A.F. Funding: E.R., S.K. All authors have read and agreed to the published version of the manuscript.

**Funding:** National Sciences and Engineering Research Council of Canada (NSERC), INNOV-R, and Prima Québec.

**Data Availability Statement:** Data is available through the corresponding author upon reasonable request.

**Acknowledgments:** The authors acknowledge the support of the industrial partner, Pyrovac Inc., Saint-Lambert de Lauzon (Québec, Canada), for supporting this research project and the supply of the recycled carbon black. The financial contribution of the National Sciences and Engineering Research Council of Canada (NSERC), INNOV-R, and Prima Québec, is also greatly appreciated.

**Conflicts of Interest:** The authors declare no potential conflicts of interest with respect to the research, authorship, and/or publication of this article.

### Abbreviations

CB	carbon black
rCB	recycled carbon black
HDPE	high-density polyethylene
TSE	twin-screw extruder
HR-TEM	high resolution transmission microscopy
EDS-X	energy dispersive X-ray spectroscopy
ATR	attenuated total reflectance
FTIR	Fourier transformed infrared spectroscopy
Fe	exposed face
Fne	non-exposed face
CI	carbonyl index
u.a.	unity of absorbance

### References

1. Sienkiewicz, M.; Kucinska-Lipka, J.; Janik, H.; Balas, A. Progress is used types management in the European Union: A review. *Waste Manag.* **2012**, *32*, 1742–1751. [[CrossRef](#)]
2. Hoang, A.T.; Nguyen, T.H.; Nguyen, H.P. Scrap tire pyrolysis as a potential strategy for waste management pathway: A review. *Energy Sources Part A Recovery Util. Environ. Eff.* **2020**, *46*, 6305–6322.
3. Martinez, J.D.; Puy, N.; Murillo, R.; Garcia, T.; Navarro, M.V.; Mastral, A.M. Waste tyre pyrolysis—A review. *Renew. Sustain. Energy Rev.* **2013**, *23*, 179–213. [[CrossRef](#)]
4. ADEME. *Pneumatiques—Données 2020*; ADEME: Angers, France, 2020; p. 58.
5. ACARP. *Rapport Annuel 2021 de l'Association Canadienne des Agences de Recyclage des Pneus*; ADEME: Angers, France, 2021; p. 22.
6. USTMA. *2019 US Scrap Tire Management Summary*; USTMA: Washington, DC, USA, 2019; p. 20.
7. Xu, J.; Yu, J.; Xu, J.; Sun, C.; He, W.; Huang, J.; Li, G. High-value utilization of waste tires: A review with focus on modified carbon black from pyrolysis. *Sci. Total Environ.* **2020**, *742*, 140235. [[CrossRef](#)] [[PubMed](#)]
8. Williams, P.T. Pyrolysis of waste tyres: A review. *Waste Manag.* **2013**, *33*, 1714–1728. [[CrossRef](#)]
9. Roy, C.; Chaala, A.; Darmstadt, H.; de Caumia, B.; Pakdel, H.; Yang, J. Conversion of used tires to carbon black and oil by pyrolysis. In *Rubber Recycling*; CRC Press: Boca Raton, FL, USA; Taylor & Francis Group, LLC.: Abingdon, UK, 2005; p. 528.
10. Deveci, S.; Antony, N.; Eryigit, B. Effect of carbon black distribution on the properties of polyethylene pipes—Part 1: Degradation of post yield mechanical properties and fracture surface analyses. *Polym. Degrad. Stab.* **2018**, *148*, 75–85. [[CrossRef](#)]
11. Wallder, V.T.; Clarke, W.J.; Decoste, J.B.; Howard, J.B. Weathering Studies on Polyethylene. *Ind. Eng. Chem.* **1950**, *42*, 2320–2325. [[CrossRef](#)]
12. Horrocks, A.R.; Mwila, J.; Miraftab, M.; Liu, M.; Chohan, S.S. The influence of carbon black on properties of orientated polypropylene 2. Thermal and photodegradation. *Polym. Degrad. Stab.* **1999**, *65*, 25–36. [[CrossRef](#)]
13. Crump, E.L. *Economic Impact Analysis for the Proposed Carbon Black Manufacturing NESHA*; U.S. Environmental Protection Agency (EPA): North Carolina, CA, USA, 2000; p. 19.
14. Ecoinvent. Ecoinvent v3.6 Database. Available online: <https://ecoinvent.org> (accessed on 1 April 2022).

15. Roy, C.; Labrecque, B.; De Caumia, B. Recycling of scrap tires to oil and carbon black by vacuum pyrolysis. *Resour. Conserv. Recycl.* **1990**, *4*, 203–213. [CrossRef]
16. LRCCP. *Biproof—Rapports axe Recyclage*; LRCCP: Vitry-sur-Seine, France, 2018.
17. Li, S.-Q.; Yao, Q.; Chi, Y.; Yan, J.-H.; Cen, K.-F. Pilot-Scale Pyrolysis of Scrap Tires in a Continuous Rotary Kiln Reactor. *Ind. Eng. Chem. Res.* **2004**, *43*, 5133–5145. [CrossRef]
18. Sahouli, B.; Blacher, S.; Brouers, F.; Darmstadt, H.; Roy, C.; Kaliaguine, S. Surface morphology and chemistry of commercial carbon black and carbon black from vacuum pyrolysis of used tyres. *Fuel* **1996**, *75*, 1244–1250. [CrossRef]
19. Roy, C.; Darmstadt, H. Carbon blacks recovered from rubber waste by vacuum pyrolysis—Comparison with commercial grades. In Proceedings of the International Conference on Rubbers, Calcutta, India, 12–14 December 1998; pp. 341–345.
20. Thomas, J.; Patil, R. The Road to Sustainable Tire Materials: Current State-of-the-Art and Future Prospectives. *Environ. Sci. Technol.* **2023**, *57*, 2209–2216. [CrossRef] [PubMed]
21. Environmental, F. Solar Radiation and Photosynthetically Active Radiation. Available online: <https://www.fondriest.com/environmental-measurements/parameters/weather/photosynthetically-active-radiation/> (accessed on 1 February 2022).
22. Gijsman, P.; Meijers, G.; Vitarelli, G. Comparison of the UV-degradation chemistry of polypropylene, polyethylene, polyamide 6 and polybutylene terephthalate. *Polym. Degrad. Stab.* **1999**, *65*, 433–441. [CrossRef]
23. Furneaux, G.C.; Ledbury, K.J.; Davis, A. Photo-oxidation of thick polymer samples—Part 1: The variation of photo-oxidation with depth in naturally and artificially weathered low density polyethylene. *Polym. Degrad. Stab.* **1981**, *3*, 431–442. [CrossRef]
24. Tüdos, F.; Iring, M. Polyolefine oxidation: Rates and products. *Acta Polym.* **1988**, *39*, 19–26. [CrossRef]
25. Gardette, M.; Perthue, A.; Gardette, J.-L.; Janecska, T.; Foldes, E.; Pukanszky, B.; Therias, S. Photo- and thermal-oxidation of polyethylene: Comparison of mechanisms and influence of unsaturation content. *Polym. Degrad. Stab.* **2013**, *98*, 2383–2390. [CrossRef]
26. Yousif, E.; Haddad, R. Photodegradation and photostabilization of polymers, especially polystyrene: A review. *SpringerPlus* **2013**, *2*, 398–430. [CrossRef]
27. Mwila, J.; MirafTAB, M.; Horrocks, A.R. Effect of carbon black on the oxidation of polyolefins—An overview. *Polym. Degrad. Stab.* **1994**, *44*, 351–356. [CrossRef]
28. Hawkins, W.L.; Hansen, R.H.; Matreyek, W.; Winslow, F.H. The effect of carbon black on thermal antioxidants for polyethylene. *J. Appl. Polym. Sci.* **1959**, *1*, 37–42. [CrossRef]
29. Zhang, J.; Liu, H.; Sablani, S.S.; Wu, Q. Recycling Functional Fillers from Waste Tires for Tailored Polystyrene Composites: Mechanical, Fire Retarding, Electromagnetic Field Shielding, and Acoustic Insulation Properties—A Short Review. *Materials* **2024**, *17*, 2675. [CrossRef]
30. Diby, I.C.P.; Belkhir, N.; Nohair, B.; Kazeruni, M.; Ruiz, E.; Kaliaguine, S. HDPE crystalline lamellae in composites involving pyrolytic carbon black: Effect on elastic modulus. *Polym. Compos.* **2024**. [CrossRef]
31. Chemicals, D. *DOW DMDA-8904 NT 7 High Density Polyethylene Resin—Technical Information*; Dow Chemicals: Garland, TX, USA, 2018.
32. Billotte, C.; Romana, L.; Flory, A.; Kaliaguine, S.; Ruiz, E. Recycled from waste tires carbon black/high-density polyethylene composite: Multi-scale mechanical properties and polymer aging. *Polym. Compos.* **2024**, *45*, 11605–11618. [CrossRef]
33. Billotte, C. Optimisation et Valorisation du Noir de Carbone de la Pyrolyse des Pneus Usés Dans Un Composite Polymère Pour Une Application en Climat Tropical. Ph.D. Thesis, Polytechnique Montréal, Montréal, QC, Canada, 2023. Available online: <https://publications.polymtl.ca/10704/> (accessed on 24 March 2023).
34. Carrasco, F.; Pagès, P.; Pascual, S.; Colom, X. Artificial aging of high-density polyethylene by ultraviolet irradiation. *Eur. Polym. J.* **2001**, *37*, 1457–1464. [CrossRef]
35. Donnet, J.-B. Structure and Reactivity of Carbon. *Tanso* **1977**, *88*, 12–33. [CrossRef]
36. Ono, K.; Yanak, M.; Tanaka, S.; Saito, Y.; Aoki, H.; Fukuda, O.; Aoki, T.; Yamaguchi, T. Influence of furnace temperature and residence time on configurations of carbon blacks. *Chem. Eng. J.* **2012**, *200–202*, 541–548. [CrossRef]
37. Hjelm, R.P.J.; Wampler, W.A.; Seeger, P.A.; Gerspacher, M. The microstructure and morphology of carbon black: A study using small angle neutron scattering and contrast variation. *J. Mater. Res.* **1994**, *9*, 3210–3222. [CrossRef]
38. Medalia, A.I. Morphology of Aggregates—VI. Effective volume of aggregates of carbon black from electron microscopy; application to vehicle absorption and to die swell of filled rubber. *J. Colloid Interface Sci.* **1970**, *22*, 115–131. [CrossRef]
39. Pertin, T. Etude d’une Matrice Thermoplastique Sous Contraintes Environnementales Tropicales: Approche Multi-Échelle. Ph.D. Thesis, Université des Antilles, Pointe-à-Pitre, France, 2022.
40. Yakimets, I.; Lai, D.; Guigon, M. Effect of photo-oxidation cracks on behaviour of thick polypropylene samples. *Polym. Degrad. Stab.* **2004**, *86*, 59–67. [CrossRef]
41. Liu, M.; Horrocks, A.R. Effect of Carbon Black on UV stability of LLDPE films under artificial weathering conditions. *Polym. Degrad. Stab.* **2002**, *75*, 485–499. [CrossRef]
42. Pertin, T.; Minatchy, G.; Adoue, M.; Flory, A.; Romana, L. Investigation of nanoindentation as a fast characterization tool for polymer degradation study. *Polym. Test.* **2019**, *81*, 106194. [CrossRef]
43. Yang, R.; Liu, Y.; Zhang, D. Spatial Heterogeneity of Photo-Oxidation and Its Relation With Crack Propagation in Polyethylene Composites. *Polym. Eng. Sci.* **2008**, *48*, 2270–2276. [CrossRef]

44. Krishnaswamy, R.K.; Yang, Q.; Fernandez-Ballester, L.; Kornfield, J.A. Effect of the Distribution of Short-Chain Branches on Crystallization Kinetics and Mechanical Properties of High-Density Polyethylene. *Macromolecules* **2008**, *41*, 1693–1704. [[CrossRef](#)]
45. Stark, N.M.; Matuana, L.M. Surface chemistry changes of weathered HDPE/wood-flour composites studied by XPS and FTIR spectroscopy. *Polym. Degrad. Stab.* **2004**, *86*, 1–9. [[CrossRef](#)]
46. Tidjani, A. Comparison of formation of oxidation products during photo-oxidation of linear low density polyethylene under different natural and accelerated weathering conditions. *Polym. Degrad. Stab.* **2000**, *68*, 465–469. [[CrossRef](#)]
47. Grause, G.; Chien, M.-F.; Inoue, C. Changes during the weathering of polyolefins. *Polym. Degrad. Stab.* **2020**, *181*, 109364. [[CrossRef](#)]
48. Douminge, L. Étude du Comportement du Polyéthylène Haute Densité Sous Irradiation Ultraviolette Ou Sollicitation Mécanique Par Spectroscopie de Fluorescence. Ph.D. Thesis, Université de La Rochelle, La Rochelle, France, 2010.
49. Almond, J.; Sugumaar, P.; Wenzel, M.N.; Hill, G.; Wallis, C. Determination of the carbonyl index of polyethylene and polypropylene using specified area under band methodology with ATR-FTIR spectroscopy. *e-Polymers* **2020**, *20*, 369–381. [[CrossRef](#)]
50. Richaud, E.; Verdu, J. *Viellissement Chimique des Polymères—Cinétique de Dégradation*; AM3152 V1; Technique de l'ingénieur: Saint-Denis, France, 2011.
51. Cunliffe, A.V.; Davis, A. Photo-oxidation of thick polymer samples—Part II: The influence of oxygen diffusion on the natural and artificial weathering of polyolefins. *Polym. Degrad. Stab.* **1982**, *4*, 17–37. [[CrossRef](#)]

**Disclaimer/Publisher's Note:** The statements, opinions and data contained in all publications are solely those of the individual author(s) and contributor(s) and not of MDPI and/or the editor(s). MDPI and/or the editor(s) disclaim responsibility for any injury to people or property resulting from any ideas, methods, instructions or products referred to in the content.